

On achieving pure electromagnetic left-handedness through magnetodielectric field compression

Loïc Markley*

School of Engineering, University of British Columbia, Kelowna, BC, Canada

(Received 11 November 2015; revised manuscript received 22 July 2016; published 8 August 2016)

The relationship between electromagnetic phase and power flow in metamaterials composed of periodic magnetodielectric inclusions is investigated. The distribution of Poynting vectors in k space across multiple Brillouin zones suggests that backward phase is a result of field compression within the inclusions, and that left-handedness can be achieved without negative electric or magnetic susceptibility (i.e., without out-of-phase dipole moments). This hypothesis is verified by showing that a one-dimensional periodic array of magnetodielectric slabs can be designed to mimic the properties of an ideal (homogeneous) left-handed medium. Furthermore, using exact fields and without any field averaging, it is shown that the structure can be designed such that practically all power is carried in the fundamental left-handed spectral component. In the limit where the fundamental contains all the power, this periodic structure has the same spectral power signature as that of a homogeneous left-handed medium. It is shown that this congruence does not manifest when the inclusions are purely dielectric, nor does it manifest for magnetodielectric inclusions in two or three dimensions.

DOI: [10.1103/PhysRevB.94.085108](https://doi.org/10.1103/PhysRevB.94.085108)**I. INTRODUCTION**

The handedness of an electromagnetic plane wave defines the relative orientations of its electric field \mathbf{E} , magnetic field \mathbf{H} , and wave vector \mathbf{k} . A medium has a left-handed response if it supports plane waves in which $(\mathbf{E}, \mathbf{H}, \mathbf{k})$ form a left-handed triplet. These waves propagate with opposing phase and group velocities (backward waves) and can give rise to counterintuitive effects such as negative refraction at an interface [1–3].

A homogeneous medium is left-handed if and only if it has simultaneous negative permittivity and negative permeability. This condition, however, has never been observed in naturally occurring materials. Although handedness cannot be rigorously defined for waves propagation through a heterogeneous medium (since these waves are not plane waves and cannot be represented by a single wave vector), the combination of metals and dielectrics in periodic structures called metamaterials has been shown to elicit macroscopic wave phenomena that mimic some characteristics of left-handed plane waves [4–12].

When the metamaterial features are highly subwavelength, the resemblance to a left-handed medium is often described by using field averaging techniques to map the electromagnetic fields to an equivalent plane wave, and then conferring the properties of the plane wave to the metamaterial. With sophisticated averaging, this process can be used to approximate the heterogeneous material properties of the structure with those of a homogeneous effective medium, a process known as homogenization [13–16].

Metamaterials with left-handed homogenized parameters have achieved negative effective permittivity and negative effective permeability through two mechanisms: the intrinsic properties of constituent materials and the macroscopic dipole moments arising from the unit cell geometry. For example, metals at microwave frequencies have an intrinsic negative permittivity at the atomic level [17], while split-ring resonators introduce macroscopic magnetic dipole moments at the unit cell

level [18,19]. In the latter case, these magnetic moments act collectively to produce negative effective permeability without constituent magnetic materials, a phenomenon that has been reported across a range of metamaterial geometries [4,20–24]. In order to distinguish between the different physical mechanisms that lead to negative effective parameters, it is useful to move beyond homogenization techniques towards methods that analyze the complete fields. Homogenization is a powerful tool to understand the macroscopic wave response of a metamaterial, however it is ultimately an approximation that discards the detailed spatial variation of the fields across each unit cell.

In this paper a metamaterial composed of periodic magnetodielectric (MD) inclusions (i.e., inclusions with both an electric $\epsilon_r > 1$ and magnetic $\mu_r > 1$ response) is investigated by expanding the electromagnetic fields of a propagating mode into a complete set of spatial frequency components and analyzing power flow in the corresponding k -space domain [25]. It is shown that opposing phase and power flow can be achieved in a one-dimensional (1D) (layered) magnetodielectric structure, without relying on intrinsic negative susceptibilities or macroscopic dipole moments. Instead, high-index MD inclusions compress the field oscillations in the direction of propagation (shrink the wavelength), with phase wrapping over each unit cell producing an effective backwards phase over the inclusion lattice.

Furthermore, it is shown that the spatial power spectrum of the metamaterial approaches that of an ideal homogeneous left-handed medium as the periodicity of the structure goes to zero and the left-handed fundamental spatial component dominates the spectrum. This congruence between the power spectrum of the metamaterial and that of a homogeneous left-handed medium is very unusual and does not typically appear in other metamaterials that are known to exhibit left-handed behavior. Interestingly, this result does not extend to two-dimensional (2D) (cylindrical) or three-dimensional (3D) (spherical) inclusions; in these structures the power remains primarily in high-order right-handed spatial frequency components as the periodicity decreases. Finally, it is shown that in nonmagnetic media, individual spectral components

*loic.markley@ubc.ca

are always right-handed and the complete power spectrum can never approach that of an ideal homogeneous left-handed medium. In these structures, power is always distributed across multiple plane-wave components and handedness is not always clearly defined.

The metamaterial under investigation is not to be confused with a photonic crystal [9,26]. Although there are topological similarities, the dielectric inclusions in the metamaterial are strongly magnetic and the lattice spacing is orders of magnitude smaller. As a consequence, the electromagnetic behavior is distinct from that of a photonic crystal and more consistent with other well-studied metamaterial structures [4,8] where power is distributed over multiple spatial frequency components in Brillouin zones adjacent to the fundamental. The significance of lattice spacing is made clear when the periodicity is increased to the order of a wavelength (well outside the metamaterial regime)—the electromagnetic behavior smoothly changes to resemble that of a photonic crystal with a single dominant high-order right-handed spatial frequency component.

The paper is organized into four main sections: Sections II and III introduce magnetodielectric field compression through a study of 1D periodic layered structures based first on magnetodielectric and then on nonmagnetic dielectric layers, Sec. IV studies 2D periodic structures with cylindrical magnetodielectric inclusions, and Sec. V studies 3D periodic structures with spherical magnetodielectric inclusions. Numerical results for 1D layered geometries are calculated using analytic equations, while 2D and 3D geometries are simulated using the full-wave finite-element solver provided in COMSOL Multiphysics [27].

II. MAGNETODIELECTRIC LAYERED STRUCTURE

It is well known from Floquet theory that a time harmonic wave propagating through a periodic structure of periodicity a with time dependence $e^{j\omega t}$ can be written in the form $f(x) = e^{-jk_F x} u(x)$, where $u(x)$ is periodic over a and $e^{-jk_F x}$ is the Floquet wave [28]. The Floquet wave vector k_F is the smallest wave vector that satisfies the periodicity of the structure. For a given wave it is equal to the minimum absolute phase difference across a unit cell divided by the periodicity a . When the periodicity of the structure is much smaller than the wavelength, the phase of the Floquet wave is the same as the phase of the wave propagating through the homogenized effective medium.

Typically, metamaterials achieve backward Floquet phase by introducing electric and magnetic dipole moments that are out of phase with the electric and magnetic fields, respectively. For example, free electrons in metals [17], capacitive loops [18], and plasmonic interfaces [23] can all contribute to out-of-phase dipole moments. When these moments are averaged over space, they produce homogenized \mathbf{D} and \mathbf{B} fields that are out of phase with the homogenized \mathbf{E} and \mathbf{H} fields, leading to opposing directions of total power flow and Floquet phase propagation. In this paper, however, backward Floquet phase is achieved using a method that does not rely on out-of-phase dipole moments.

Consider a wave with a Floquet wave vector k_F propagating through a periodic medium of periodicity $a \ll \lambda$. This wave would typically be interpreted as having a small phase delay

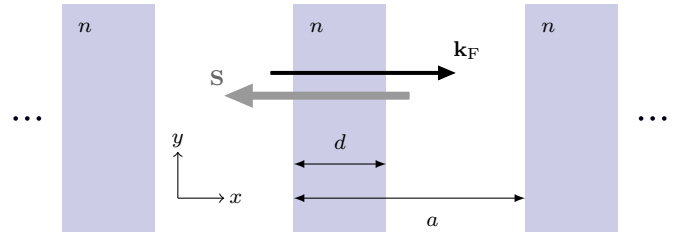


FIG. 1. A diagram of the magnetodielectric layered structure. An electromagnetic wave propagates through the layers with Floquet phase propagating in the positive x direction and power flowing in the negative x direction.

across each unit cell of $\phi_{\text{delay}} = k_F a$. Due to the periodicity of time harmonic signals, however, this phase delay could alternatively be viewed as a large phase advance across each unit cell of $\phi_{\text{advance}} = 2\pi - k_F a$. Although both ϕ_{delay} and ϕ_{advance} correspond to the same Floquet wave vector due to phase wrapping, the former implies slow spatial phase variation in the direction of k_F while the latter implies fast spatial phase variation in the opposite direction. It is therefore possible to obtain a backwards Floquet phase delay by inserting a sufficiently high-index layer of magnetodielectric material into each unit cell. These layers would serve to compress the fields along the axis of propagation and produce the high spatial phase advance equivalent to the Floquet phase delay.

To investigate this phenomenon in detail, consider a periodic structure consisting of alternating air and magnetodielectric layers as illustrated in Fig. 1. The MD layers have a refractive index of n and thickness d , and are spaced along x with periodicity a . Consider a wave propagating parallel to the x axis (normal to the layers) with a Floquet wave propagating in the positive x direction and power flow in the negative x direction. If the MD layers are matched to free space ($\epsilon_r = \mu_r = n$), there will be no reflections at any of the interfaces, and the wave will be a pure traveling wave with a uniform amplitude throughout the structure.

In order for power to flow in the negative x direction, the waves within each layer must also propagate in the negative x direction. If the fields are polarized in the y direction and $k = \omega/c$ is the wave vector in free space, the complete electric and magnetic fields are given by the following expressions:

$$E_y(x) = \begin{cases} E_0 e^{jk\xi - jk_F qa}, & 0 \leq \xi < a - d, \\ E_0 e^{jkn\xi - jk_F qa}, & -d \leq \xi < 0, \end{cases} \quad (1)$$

$$H_z(x) = \frac{1}{\eta_0} E_y(x), \quad (2)$$

where $q = (x \text{ div } a)$ and $\xi = (x \text{ mod } a)$ are the quotient and remainder of x/a such that $x = qa + \xi$. The fields within the MD layers vary with a phase term $e^{jkn\xi}$ and the fields between the MD layers vary with a phase term $e^{jk\xi}$. In order to ensure that the Floquet wave propagates in the positive x direction with phase $e^{-jk_F x}$, the total per-unit-cell phase delay ϕ must

satisfy

$$\phi = k_F a = -k(a - d) - knd + 2\pi p, \quad (3)$$

where p is any integer. Since k_F is positive, the phase delay will fall within the range $0 < \phi < \pi$, where $\phi = \pi$ corresponds to the edge of the first Brillouin zone.

If the complete fields are considered without approximation or homogenization, the question of this structure's handedness is an intriguing one. Both constituent materials are intrinsically right-handed, yet opposing power and Floquet phase would suggest a left-handed effective homogeneous medium. In the Introduction, handedness was rigorously defined for a single plane wave where the direction of phase propagation was uniquely determined by the wave vector. A mode propagating through an inhomogeneous medium, however, cannot be expressed as a single plane wave and therefore cannot be assigned a single wave vector. This makes the direction of phase propagation ambiguous and implies that a single binary parameter like handedness is not appropriate to characterize the complete inhomogeneous vectorial relationship between phase and power flow.

Although homogenization techniques provide a powerful tool for modeling the macroscopic behavior of periodic structures and metamaterials, they provide a limited view of phase and power flow within a propagating wave. Sampling the field at lattice intervals or averaging the fields across unit cells discards information about the local field distributions within unit cells that is critical to understand how power is distributed across multiple Brillouin zones in k space. Conventional wave vector diagrams use phase matching across equifrequency contours to calculate directions of refraction and reflection. In periodic structures, the folding of higher order Brillouin zones into the first Brillouin zone enables the accurate prediction of anomalous refraction and reflection due to higher-order components [12]. Since these contours are determined only from the periodicity of propagating waves, however, high-order plane-wave components are indistinguishable from the fundamental Floquet wave, and the relationship between phase and power becomes ambiguous.

By contrast, expanding the detailed electromagnetic fields into a complete set of plane-wave components can provide a rigorous analysis of phase and power flow across all Brillouin zones [29–31]. Directions of phase propagation and power flow are associated with each plane-wave component, and handedness can be assigned to a component by component basis. A similar method was previously applied to photonic crystals in which modes were shown to have a single Fourier component from which overall right-handedness could be ascertained [29].

Let the complete expansion technique now be applied to map power density in the layered MD structure to the spatial frequency domain. This will enable a rigorous comparison to the power spectrum of an ideal homogeneous left-handed medium.

A general electromagnetic field can be mapped to the k -space domain by taking the multidimensional Fourier transform of each component [25]. When the field represents a wave propagating through a periodic structure, it expands into a Fourier series with a fundamental mode propagating with the Floquet wave vector \mathbf{k}_F . The electric and magnetic fields can

be written as

$$\mathbf{E}(\mathbf{r}) = e^{-j\mathbf{k}_F \cdot \mathbf{r}} \sum_{\mathbf{m}} \mathbf{e}_{\mathbf{m}} e^{-j\mathbf{g}_{\mathbf{m}} \cdot \mathbf{r}}, \quad (4)$$

$$\mathbf{H}(\mathbf{r}) = e^{-j\mathbf{k}_F \cdot \mathbf{r}} \sum_{\mathbf{m}} \mathbf{h}_{\mathbf{m}} e^{-j\mathbf{g}_{\mathbf{m}} \cdot \mathbf{r}}, \quad (5)$$

where the series summation is multidimensional over the indices $\mathbf{m} \equiv (m_x, m_y, m_z)$ and $\mathbf{g}_{\mathbf{m}} = 2\pi(\frac{m_x}{a_x}\hat{\mathbf{x}} + \frac{m_y}{a_y}\hat{\mathbf{y}} + \frac{m_z}{a_z}\hat{\mathbf{z}})$ is the \mathbf{m} th reciprocal lattice vector corresponding to the unit cell dimensions a_x , a_y , and a_z .

The Fourier coefficients $\mathbf{e}_{\mathbf{m}}$ and $\mathbf{h}_{\mathbf{m}}$ decompose the fields $\mathbf{E}(\mathbf{r})$ and $\mathbf{H}(\mathbf{r})$ over the points in k space described by the corresponding wave vectors $\mathbf{k}_{\mathbf{m}} = \mathbf{k}_F + \mathbf{g}_{\mathbf{m}}$. Since each wave vector is located within a different Brillouin zone, each pair of coefficients also corresponds to the contribution from a different Brillouin zone. The fundamental component \mathbf{k}_0 is equal to the Floquet wave vector \mathbf{k}_F and is located within the first Brillouin zone where $\mathbf{g}_{\mathbf{m}} = \mathbf{0}$. All other components are higher order components and are located outside the first Brillouin zone.

The time-averaged power density associated with each Fourier component in k space can be calculated using the Poynting vector

$$\mathbf{s}_{\mathbf{m}} = \frac{1}{2} \text{Re}\{\mathbf{e}_{\mathbf{m}} \times \mathbf{h}_{\mathbf{m}}^*\}, \quad (6)$$

with the total time and space averaged power density equal to the vector sum of all component Poynting vectors $\langle \mathbf{S}(\mathbf{r}) \rangle = \sum_{\mathbf{m}} \mathbf{s}_{\mathbf{m}}$. Each vector $\mathbf{s}_{\mathbf{m}}$ corresponds to a unique wave vector $\mathbf{k}_{\mathbf{m}}$, enabling the power flow to be mapped across k space. Plotting this power map provides a visual representation of the multidimensional distribution of power and phase of the complete electromagnetic field. Although handedness is not defined for the total field (since the structure is inhomogeneous in the direction of propagation), each individual component is a plane wave and can be described as right- or left-handed depending on the angle between $\mathbf{s}_{\mathbf{m}}$ and $\mathbf{k}_{\mathbf{m}}$.

Note that a traditional wave vector diagram plots the loci of all possible $\mathbf{k}_{\mathbf{m}}$ points at a given frequency (equifrequency contours) and is periodic in k space. The gradient of these contours determines the direction of total averaged power flow $\langle \mathbf{S}(\mathbf{r}) \rangle$, but no more information regarding power flow is provided. In contrast, by calculating the Fourier coefficients using (4) and (5) and plotting $\mathbf{s}_{\mathbf{m}}$ vectors on top of the equifrequency contours, the k -space diagram becomes aperiodic and the contribution of power flow from each Brillouin zone can be clearly identified. This provides additional information regarding both phase and power flow of a wave propagating through a periodic structure.

To determine the k -space mapping of the layered MD structure, the electromagnetic fields in (1) and (2) can be expanded into Fourier series using (4) and (5). Since the structure in Fig. 1 is uniform along y and z , the Fourier series in (4) and (5) reduce to 1D summations along x over a single index m . The wave vectors take the form $\mathbf{k}_m = (k_F + 2\pi m/a)\hat{\mathbf{x}}$ and the Fourier coefficients take the form $\mathbf{e}_m = e_m\hat{\mathbf{y}}$ and $\mathbf{h}_m = h_m\hat{\mathbf{z}}$. The power flow at each point in k space can then be written as $\mathbf{s}_m = \frac{1}{2} \text{Re}\{e_m h_m^*\}\hat{\mathbf{x}}$.

The Poynting vector associated with the fundamental Fourier component \mathbf{s}_0 can be normalized with respect to the

total power $\langle \mathbf{S}(x) \rangle = \sum_m \mathbf{s}_m$ and simplified to the following expression:

$$\frac{\mathbf{s}_0}{|\langle \mathbf{S}(x) \rangle|} = -\text{sinc}^2\left(\frac{(k_F + k)(a - d)}{2}\right) \times \left(\frac{2\pi p - (k_F + k)a}{2\pi p - (k_F + k)(a - d)}\right)^2 \left(\frac{a - d}{a}\right)^2 \hat{\mathbf{x}}. \quad (7)$$

The square terms in (7) indicate that \mathbf{s}_0 always points in the negative $\hat{\mathbf{x}}$ direction. Since $\mathbf{k}_0 = k_F \hat{\mathbf{x}}$ points opposite to \mathbf{s}_0 , the fundamental component of the wave propagating through the MD layered structure is always left-handed. To design the structure to mimic a homogeneous left-handed medium of index $n_{\text{eff}} = -1$, the parameter k_F can be set equal to k , with $p = 1$ to ensure the smallest possible index of refraction. Following from (3), the magnetodielectric index of refraction is then given by

$$n = 1 + \frac{\lambda - 2a}{d}. \quad (8)$$

Figure 2 plots the x component of the computed power distribution $\mathbf{s}_0/\langle \mathbf{S}(x) \rangle$ in k space for three MD layer configurations. The structure properties vary only in the x direction so the Poynting vectors in k space all lie along the k_x axis. Because the MD layers are perfectly impedance matched and there are no reflections, the electric and magnetic fields are

in-phase and power only flows in the negative x direction. All components with $k_x > 0$ (including the fundamental) are therefore left-handed while all the components with $k_x < 0$ are right-handed. As the unit cell size is made smaller and the MD layers are made thinner, the distribution of power moves from residing primarily within right-handed Fourier components outside the first Brillouin zone to residing primarily within the fundamental left-handed component inside the first Brillouin zone.

The first multilayer configuration (shown in blue in the upper row of Fig. 2) has a unit cell size of $a = 0.2\lambda$, MD layer thickness of $d = 0.75a$, and refractive index of $n = 5$. The second configuration (shown in green in the middle row of the figure) has $a = 0.2\lambda$, $d = 0.35a$, and $n = 23.9$. The third configuration (shown in red in the lower row of the figure) has $a = 0.05\lambda$, $d = 0.1a$, and $n = 181$. As the unit cell size decreases, higher index layers are required to compress the field oscillations (reduce the guided wavelength) sufficiently within each unit cell to achieve phase wrapping. As both the unit cell size a and MD layer filling factor d/a decreases, the power in the higher order leftward-propagating (right-handed) component diminishes and the power in the fundamental rightward-propagating (left-handed) component increases. In the upper layer configuration, most of the fields are located within the MD medium, and the phase variation is consistent with that of a plane wave outside the first Brillouin zone. In the lower configuration, however, the unit cells are small,

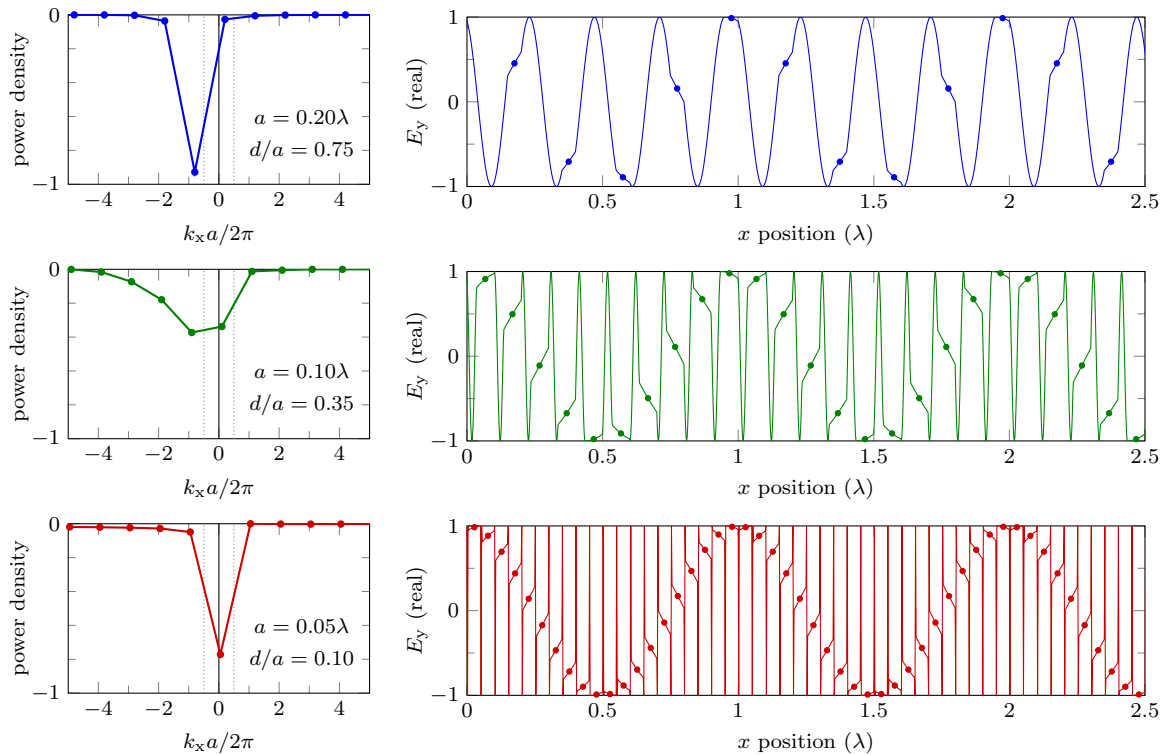


FIG. 2. The 1D normalized power spectrum $s_{x,m}/|\langle \mathbf{S}_x(x) \rangle|$ is plotted alongside a snapshot of the electric field for three matched $\epsilon_r = \mu_r = n$ layer configurations. The $m = -1$ component ($k_x a / 2\pi \approx -1$) dominates the spectrum at large unit cell sizes and large filling factors (upper configuration), while the $m = 0$ component ($k_x a / 2\pi \approx 0$) dominates the spectrum when both are small (lower configuration). The first Brillouin zone is indicated in the power density plots by the vertical dotted lines. Dots are placed in the field plots at lattice intervals to highlight the Floquet phase (which corresponds to the fundamental Fourier component). Over the time evolution of the fields, the dots forming the Floquet wave propagate to the right, while the fields in each narrow region propagate to the left.

most of the fields are located in air, and the phase variation is consistent with a fundamental left-handed plane wave. To put this into context, the normalized power density spectrum of an ideal left-handed homogeneous medium would contain a single nonzero point that would be located inside the first Brillouin zone with a value of -1 .

It is clear from Fig. 2 that a wave propagating through a layered MD medium matched to free space will have a power spectrum that is dominated by the $m = 0$ or $m = -1$ Fourier components. The contribution of each of these components to the total power can be calculated directly using the following two expressions:

$$\frac{s_0}{|\langle \mathbf{S}(x) \rangle|} = -\frac{\sin^2[k(a-d)](\pi - ka)^2}{k^2 a^2 [\pi - k(a-d)]^2} \hat{\mathbf{x}}, \quad (9)$$

$$\frac{s_{-1}}{|\langle \mathbf{S}(x) \rangle|} = -\frac{\sin^2[k(a-d) + \pi d a^{-1}] a^2}{(a-d)^2 (\pi - ka)^2} \hat{\mathbf{x}}, \quad (10)$$

where (9) is simplified from (7) by setting $k_F = k$ ($n_{\text{eff}} = -1$) and $p = 1$, and (10) was derived independently. Both these functions are monotonic with respect to a and d/a . When both a and d/a are small, most of the power is contained within the $m = 0$ mode. When either one is large, the power is primarily in the $m = -1$ mode.

Using (9) and (10), the 50% to 90% power contours for the $m = 0$ and $m = -1$ Fourier components are plotted together in Fig. 3 over a range of unit cell sizes a and MD-layer filling factors d/a . Since only one component can carry more than 50% of the total power for any given geometry, these contours do not overlap and each set of contours appears over a region that is independent from the other. The $m = 0$ contours appear

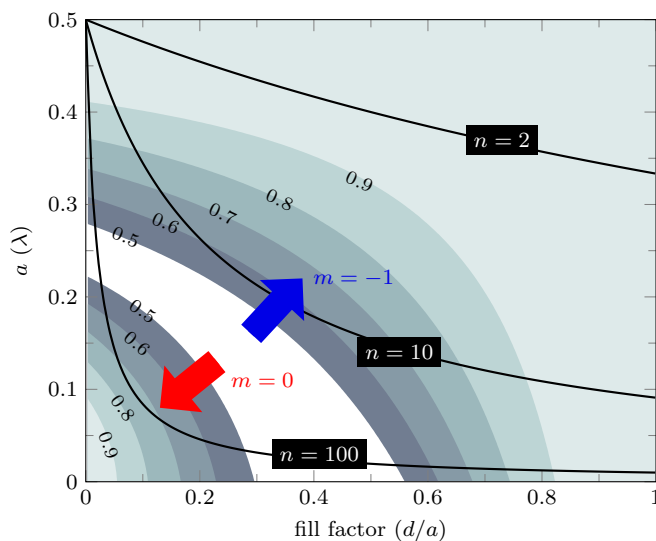


FIG. 3. The fractional power in the $m = 0$ (bottom left of the figure, indicated by the red arrow) and $m = -1$ (top and right of the figure, indicated by the blue arrow) components are plotted as a function of periodicity a and fill factor d/a . Contours are plotted at 10% intervals for each component from 50% to 90%. The corresponding index of refraction given by $n = 1 + (\lambda - 2a)/d$ increases towards the bottom left of the figure. The three solid black lines indicate the index contours for $n = 2$, $n = 10$, and $n = 100$.

at the bottom left corner of the figure (indicated by the red arrow) while the $m = -1$ contours cover most of the upper right three quadrants (indicated by the blue arrow). The white region between the two sets of contours indicates the region where no single Fourier component dominates the spectrum. An index of refraction value is also associated with each layer geometry. Three index contours are plotted in the figure (for $n = 2$, $n = 10$, and $n = 100$), showing index values that get larger towards the bottom left corner of the figure. This is consistent with (8), which states that as d becomes very small, larger and larger values of n are required to maintain the field compression necessary for $n_{\text{eff}} = -1$.

As $a \rightarrow 0$ and $d/a \rightarrow 0$, the fraction of power carried by the $m = 0$ Fourier component increases towards unity. The electromagnetic fields from this Fourier component were shown earlier to be left-handed, and are equivalent to those of the wave that propagates through a matched $n = -1$ homogeneous medium. In the limit where $a \rightarrow 0$, the fractional power within the $m = 0$ component has the form $|s_0/\langle \mathbf{S}(x) \rangle| \rightarrow (1 - d/a)^2$. In the limit where d/a also goes to zero, all the power carried in the complete electromagnetic field is contained within the fundamental Fourier component, and the spatial power spectrum is identical to that of a wave propagating through an ideal homogeneous left-handed medium. To the best of our knowledge, this congruence between power spectra has never been observed in other metamaterials. Left-handedness has only been reported with respect to the homogeneous effective medium representations of other structures, i.e., after field averaging has been performed [32]. Although a set of homogenized parameters may suggest that $n_{\text{eff}} = -1$, this does not mean that the spatial power spectrum of the complete field is congruent with that of an ideal homogeneous left-handed medium. In fact, this is typically not the case. The power spectrum of the MD layered structure, however, does approach that of the homogeneous left-handed medium in the limit where the unit cell size and filling factor goes to zero. Furthermore, it must be stressed that this structure achieves a left-handed power spectrum without using negative susceptibility materials (such as metals) nor by introducing out-of-phase dipole moments. Left-handedness arises through longitudinal compression of the electromagnetic wave (from the high-index MD layers) which results in phase wrapping over each unit cell. A similar effect was observed in negative-refractive-index transmission lines where high-reactive loading was used to achieve arbitrarily pure backward waves [33].

III. NONMAGNETIC INCLUSIONS

The previous section demonstrated how field compression within periodic inclusions can lead to left-handed wave propagation when the unit cell size and filling factor are very small. Magnetodielectric layers that were matched to free space were considered in that study. This raises an important question: if nonmagnetic inclusions were used instead (with $\epsilon_r = n^2$ and $\mu_r = 1$), would the same left-handed spectrum be achieved? The electromagnetic fields would still be compressed in the direction of propagation, however mismatch at every interface would introduce reflected waves that could lead to a very different spatial power spectrum.

When the structure is purely dielectric (nonmagnetic), the handedness of each Fourier component can actually be determined *a priori*. Substituting (4) and (5) into Faraday's law and taking the inner product with respect $e^{j\mathbf{k}_m \cdot \mathbf{r}}$ reveals the following relationship between \mathbf{e}_m and \mathbf{h}_m :

$$\mathbf{k}_m \times \mathbf{e}_m = \omega\mu_0\mathbf{h}_m. \quad (11)$$

The handedness of the m th component can be determined by evaluating the sign of $\mathbf{k}_m \cdot \mathbf{s}_m$. A positive sign would indicate right-handedness while a negative sign would indicate left-handedness. Using (6) and (11), the dot product simplifies to

$$\mathbf{k}_m \cdot \mathbf{s}_m = \frac{1}{2}\omega\mu_0|\mathbf{h}_m|^2 \geq 0, \quad (12)$$

which is always greater than or equal to zero. This means that assessed individually, each k -space component of a wave propagating through a nonmagnetic structure will always be right-handed, no matter the polarization, the geometry, or the constituent nonmagnetic materials. As a consequence, a nonmagnetic structure can never support a wave with a power spectrum that approaches that of a homogeneous left-handed medium. A wave with one dominant Fourier component will always be right-handed while left-handed wave characteristics must arise from a combination of multiple higher-order plane-wave components. Given this conclusion, what does the

spectral power distribution look like when the unit cell size and filling factor of the layered dielectric medium go to zero?

The dominance of the left-handed fundamental power spectral component in the MD layered medium relies on impedance matching between the MD layers and the air gaps. When the layers are mismatched, such as in the nonmagnetic case where $\mu_r/\epsilon_r = 1/n^2$, the power spectrum changes dramatically from the one plotted in Fig. 2. As the unit cells are made smaller, the index of refraction within the inclusions increases and the wave impedance decreases. This causes the mismatch between the dielectric and air layers to increase, resulting in larger reflections at each interface. Evidence of these reflections can be seen through the appearance of standing waves in the fields as well as through the trend towards odd symmetry in the corresponding power spectrum.

Figure 4 plots the power spectrum for three nonmagnetic layered configurations with an effective index $n_{\text{eff}} = -1$. The upper panel plots the case where the unit cell has a lattice spacing $a = 0.20\lambda$ and filling factor $d = 0.75a$. Here the corresponding index is $n = 4.57$ and most of the power is contained within the $m = -1$ component outside the first Brillouin zone. In the middle panel, $a = 0.10\lambda$ and $d = 0.35a$. The index is now $n = 16.6$ and power is distributed primarily between the $m = -1$ and $m = 1$ components (both of which are still outside the first Brillouin zone). In the lower panel, $a = 0.05\lambda$ and $d = 0.1a$. The index rises to $n = 104$ and the fundamental component still carries minimal power.

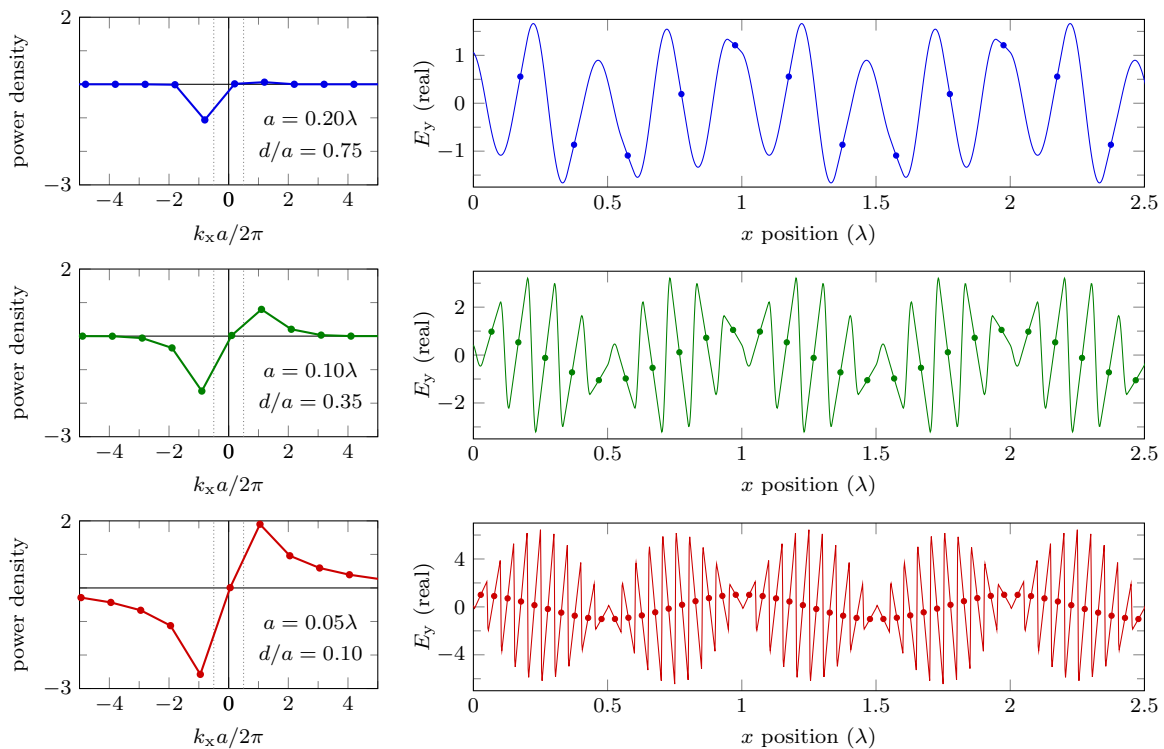


FIG. 4. The 1D normalized power spectrum $s_{x,m}/|S_x|$ is plotted alongside a snapshot of the electric field for three nonmagnetic ($\mu_r = 1$) layered configurations. The $m = -1$ component ($k_x a / 2\pi \approx -1$) dominates the spectrum at large unit cell sizes and large filling factors (upper configuration in blue), while a resonant mode builds up with strong contributions from the $m = -1$ and $m = +1$ components ($k_x a / 2\pi \approx \pm 1$) when both are small (lower configuration in red). The first Brillouin zone is indicated in the power density plots by the vertical dotted lines. Dots are placed in the field plots at lattice intervals to highlight the Floquet phase. Unlike the matched MD layer structure, very little power is ever carried in the fundamental (right-handed) component. Standing wave patterns appear as the index of refraction increases, formed by the superposition of paired $m = \pm 1$ components, with the envelope propagating in phase with the Floquet wave vector.

When the unit cell size a and filling factor d/a are large, the power appears mostly within the $m = -1$ Fourier component. This indicates that the wave closely resembles a single high-order plane wave propagating in the same direction as power flow (i.e., with a clear right-handed character). When a and d/a are small, the power is mostly distributed between the $m = \pm 1$ components and handedness is not clearly defined. Together, these individually right-handed components resemble a standing wave with a propagating Floquet wave envelope. Unlike the equivalent matched MD layer configuration, the power contained within the $m = 0$ component is virtually nonexistent. This component represents the power carries by the electric and magnetic fields averaged over the unit cell (after compensating for the Floquet phase). When it is zero, it demonstrates that the fields have little resemblance to the plane wave supported by the homogeneous effective medium representation. Instead, the fields are composed primarily of standing waves formed from high-order plane-wave components.

Similarly to the MD configurations, thinner dielectric layers require higher indices of refraction to maintain phase wrapping across each unit cell. The higher index, however, leads to greater mismatch at each interface. The mismatch leads to more pronounced standing waves which are visible in the field plots as the rapid oscillations in the field. The wave envelope propagates in the positive x direction with spatial frequency k_F while the overall net power is carried in the negative x direction. Sampling the fields at every unit cell boundary (indicated by the dots in the field plots in Fig. 4) reveals the Floquet phase within each component wave vector $k_m = k_F + 2\pi m/a$. Care should be made, however, not to confuse the presence of this dotted sinusoid with the fundamental Fourier component (which carries negligible power). Instead, it should be recognized that sampling the sum of a strong right-handed $m = 1$ mode $Ae^{-j(k_F+2\pi/a)x}$ and a strong right-handed $m = -1$ mode $Be^{-j(k_F-2\pi/a)x}$ at the unit cell boundaries $x_q = qa$ produces a discrete wave $(A+B)e^{-jk_F x_q}$ with wave vector k_F and does not imply power in the fundamental.

In summary, an electromagnetic wave propagating through a 1D periodic structure composed of purely dielectric layers will never have a power spectrum that approaches that of a left-handed homogeneous medium. Strong field compression leads to interface mismatch and large standing waves. Although it is possible to achieve power flow in the direction opposite to the Floquet phase, this phenomenon will always arise due to the contribution of high-order right-handed spatial frequency components.

IV. CYLINDRICAL MAGNETODIELECTRIC INCLUSIONS

In the 1D matched magnetodielectric layered structure, the power in the fundamental component could be made very high by decreasing the unit cell size a and fill factor d/a . Since the thin MD layers had infinite transverse extent, any wave propagating through the structure would be forced to pass through the MD material and experience field compression. Field compression led to phase wrapping over each unit cell, conferring a backward wave across the air gaps between MD layers. When the lattice spacing and fill factors were small, the backward wave dominated the spectral mapping and the

compressed fields within the MD layers had little impact on spectral power flow.

When the MD inclusions are extended to 2D (cylinders) or 3D (spheres), a given matched index n (with $\epsilon_r = \mu_r = n$) and filling ratio d/a will no longer always support a mode with opposing total power and Floquet phase. The finite transverse extent of the inclusions provides a path for the electromagnetic wave to flow around the inclusions and potentially avoid field compression altogether. Consider the 2D geometry where the cross section of each unit cell is a square of side length a , and each unit cell contains a magnetodielectric cylinder of diameter d and matched refractive index n . A mode will always exist in which the direction of local power flow inside the MD cylinder is opposite to the direction of the Floquet wave vector, but when n is high and d/a is low, the overall power flow is dominated by the fields outside the cylinders and net power is still in the forward direction.

In Fig. 5 the time evolution of the fields is plotted through a series of six snapshots of the transverse field (E_y for the TE mode). The left column plots the fields from one unit cell of a lattice of cylinders with $n = 20$ and $d = 0.2a$ while the right column plots the fields from a lattice with $n = 20$ and $d = 0.9a$. As time increases from top to bottom, the fields inside the cylinders can be observed to propagate in the negative x direction (from right to left), while the fields outside the cylinders propagate in the positive x direction (from left to

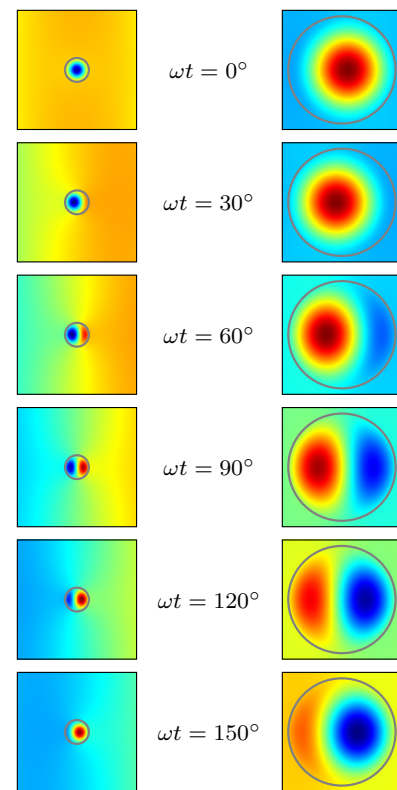


FIG. 5. Snapshots of the transverse field from two MD cylinder configurations are plotted over six time steps to illustrate the time evolution of the transverse field. The snapshots on the left correspond to $n = 20$ and $d = 0.2a$ while the snapshots on the right correspond to $n = 20$ and $d = 0.9a$.

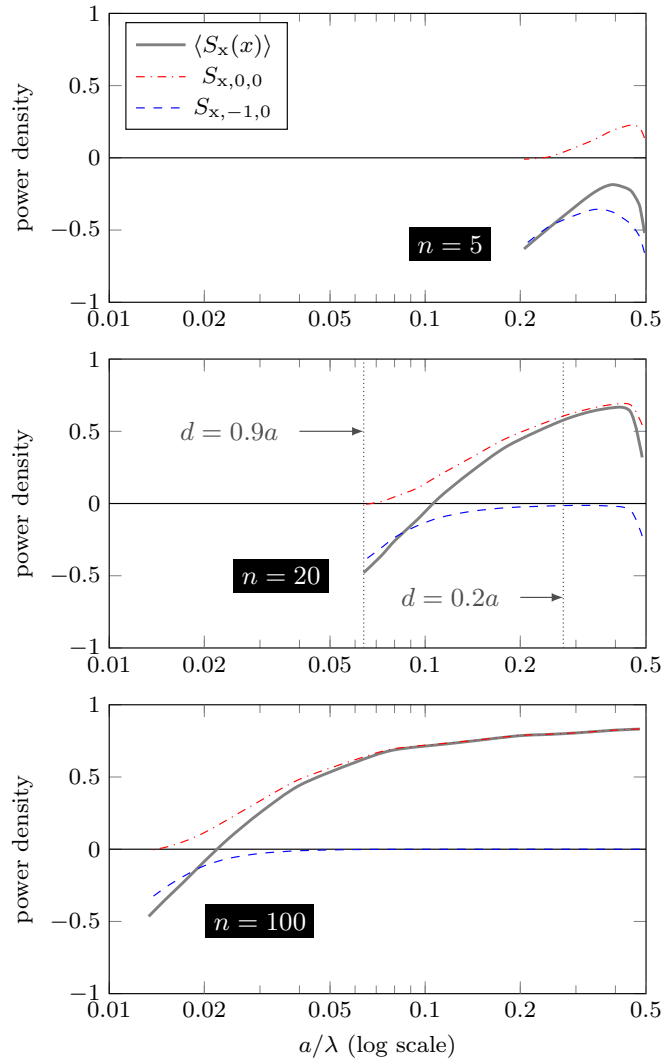


FIG. 6. The total x -directed power $\langle S_x(x) \rangle$ is plotted in solid gray for MD cylinder inclusions with three different refractive indices ($n = 5$, $n = 20$, and $n = 100$). The power is plotted as a function of lattice spacing a . The red dash-dot curve plots the power contribution of the fundamental $(0,0)$ component, while the blue dashed curve plots the contribution of the $(-1,0)$ component. The locations of the two configurations whose six time snapshots are plotted in Fig. 5 are indicated by the vertical dotted lines on the $n = 20$ plot. Note that the filling ratio d/a increases as a decreases in order to provide sufficient field compression through the high-index inclusions to ensure phase wrapping over each unit cell.

right). When the inclusions are small, such as when $d = 0.2a$, the fields outside the cylinders dominate the mode and the total power flows in the direction of Floquet phase (to the right). When the inclusions are large, however, such as when $d = 0.9a$, the fields inside the cylinders dominate the mode and total power flows opposite to the Floquet phase (to the left).

The distribution of power flow in the spatial frequency domain can be analyzed quantitatively by taking the 2D Fourier transform of the electric and magnetic fields and mapping the component Poynting vectors over the $k_x k_y$ plane. Figure 6 plots the total power flow $\langle S_x(x) \rangle = \sum_{m_x} \sum_{m_y} S_{x,m_x,m_y}$ as a function

of a for $n = 5$, $n = 20$, and $n = 100$. The contributions from the two most prominent components $(m_x, m_y) = (-1, 0)$ and $(0, 0)$ are plotted alongside. When the MD index is small, such as for $n = 5$, the backward flowing waves within the cylinders couple strongly to the outside fields, resulting in negative total power flow over the entire range of a values. This occurs even for small filling ratios d/a , however backwards power is due to the contribution of the high-order right-handed $(-1, 0)$ Fourier component. Higher MD indices, however, such as $n = 20$ and $n = 100$, have weaker coupling between the fields inside and outside the cylinders when d/a is small. The total power flow in these cases is positive since most of the power is carried in the host medium (i.e., outside the MD inclusions, see left snapshots in Fig. 5). When the inclusions are large, however, the backward flowing fields inside the MD cylinders dominate the mode, producing negative total power flow (opposing power and Floquet phase, see right snapshots in Fig. 5), but again this is due to the contribution of the high-order right-handed $(-1, 0)$ component rather than a left-handed fundamental component. For a given MD index, there is a threshold above which power flow is negative; for $n = 20$ it is $d > 0.53a$, and for $n = 100$ it is $d > 0.55a$.

The fundamental component carrying positive power dominates the spectrum when the inclusions are small (d/a is small and a is large) and the fields in the host medium dominate the mode. As the inclusions become large (d/a become large and a becomes small), however, the fields within the cylinders dominate the mode and the contribution of the fundamental component to the total power becomes negligible. The fields within the inclusions are compressed from the high index MD material and most of the power is contained within the first high-order mode at $(-1, 0)$ carrying negative power. The two vertical dotted lines in the $n = 20$ figure represent the configurations corresponding to the time snapshots from Fig. 5. When $d = 0.2a$, the negative power flow inside the inclusions is not sufficient to overcome the positive power flow outside. When $d = 0.9a$, the field compression within the inclusions causes the first order Fourier component to have the greatest contribution to the total power.

The layered structure analyzed in Sec. II was able to demonstrate a power spectrum congruent with that of a homogeneous left-handed medium. That congruence is not visible here in the case of a 2D lattice of MD inclusions. The layered structure relied on field compression within MD inclusions and phase wrapping over each unit cell to achieve backward phase propagation. Two features were critical to ensure that the left-handed fundamental component dominated the spectrum: (i) the MD inclusions needed to be thin so that the spectrum depicted the fields between the layers, not inside them; and (ii) the coupling between the fields inside and outside the MD inclusions had to be strong so the backward phase from within the inclusions would be conferred to the fields between the inclusions. In the case of cylindrical inclusions (or spherical inclusions in 3D) these two conditions cannot be achieved simultaneously. Large inclusions are necessary to achieve negative power flow, but prevent the fundamental Fourier component from contributing strongly to the total power. Likewise, small inclusions correspond to

dominant fundamental components, but most of the power is carried by the host medium in the same direction as the Floquet wave. Because these conditions are mutually exclusive in 2D (or 3D), the medium formed from an array of cylinders (or spheres) will never exhibit a power signature that approaches that of a pure left-handed medium. Backwards power will always arise from power flow contributions originating outside the first Brillouin zone. This conclusion can be extended to other topologically similar structures with finite inclusions separated in all directions by air gaps. To achieve a power spectrum with a dominant left-handed fundamental mode, the inclusions would need to extend infinitely in the transverse directions and be separated by air gaps in the direction of propagation.

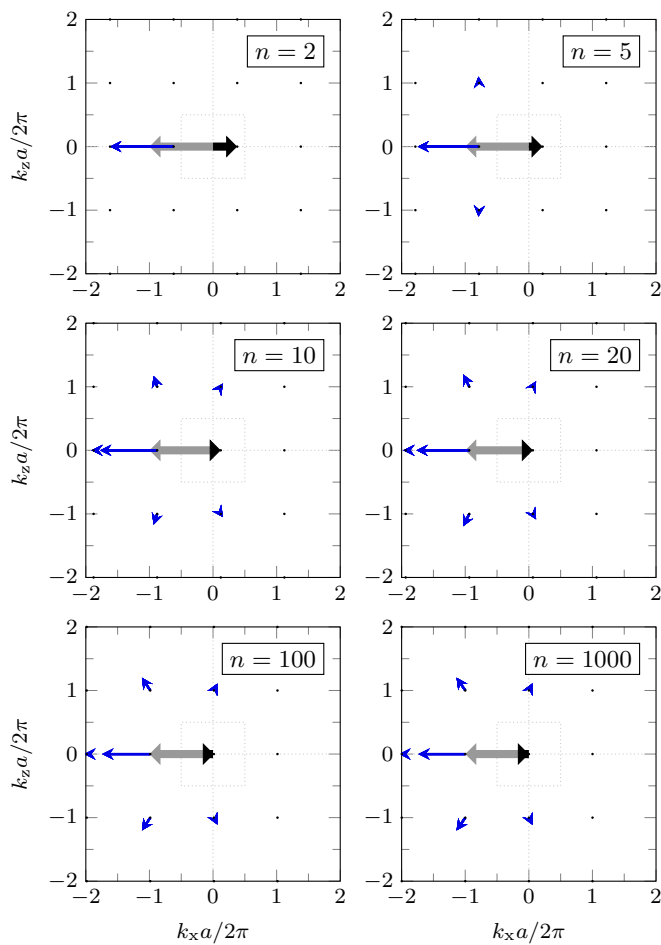


FIG. 7. The k -space maps of phase and power flow for matched MD cylindrical inclusions with $d = 0.9a$ are plotted for six different refractive indices from $n = 2$ to $n = 100$. The thick gray arrows represent the total power, while the short black arrows indicate the Floquet wave vector. The first Brillouin zone is indicated by the dashed square. As the index increases, the lattice spacing decreases, reaching $a = 0.38\lambda$ at $n = 2$, $a = 0.22\lambda$ at $n = 5$, $a = 0.12\lambda$ at $n = 10$, $a = 0.064\lambda$ at $n = 20$, $a = 0.013\lambda$ at $n = 100$, and $a = 0.0014\lambda$ at $n = 1000$. Although additional wave components appear as the index increases from $n = 2$, the $(-1, 0)$ component always dominates the power spectrum and the $(0, 0)$ contributes minimally to the total power.

The lack of congruence with a pure left-handed spectrum can be observed in Fig. 7 where the index of refraction $n = \epsilon_r = \mu_r$ is increased for a given cylinder diameter of $d = 0.9a$, producing smaller and smaller unit cells, but no convergence to a spectrum containing a single left-handed fundamental component. The fields are mapped to k space for six different refractive indices, showing how the spatial frequency distribution of power and phase changes with unit cell size. When the index is low, the host medium fields are tightly coupled to the MD medium fields, and the mode is characterized by a power spectrum dominated by the $(-1, 0)$ component. As the index of the cylinders increases, off-axis components begin to appear in the k -space power spectrum, including multiple components with $m_x = 0$. These components are secondary contributors to the total power, however, with the $(0, -1)$ component consistently carrying most of the spectral power.

Figure 8 plots the transverse fields over a large number of unit cells to illustrate the presence of the $(0, -1)$ component in two geometric configurations. The transverse electric field E_y is plotted over the xz plane for the TE modes corresponding to $n = 2$ and $n = 20$. When $n = 2$, the fields resemble that of a single right-handed plane wave propagating in the direction opposite to the Floquet wave. The apparent backwards Floquet phase is a product of aliasing due to an undersampling of the fields at the unit cell boundaries (band folding) and does not signify left-handedness. When $n = 20$, the high-order right-handed wave is still clearly visible, but now the long wavelength Floquet wave can also be seen in the background (see the black scale bar for the wavelength).

In this section, periodic structures with cylindrical magnetodielectric inclusions were studied and found to have spectra dominated by a high-order right-handed component consistent with magnetodielectric field compression. The conditions necessary for spectral congruence with a homogeneous left-handed medium were found to be incompatible with inclusions that were not infinite in transverse extent.

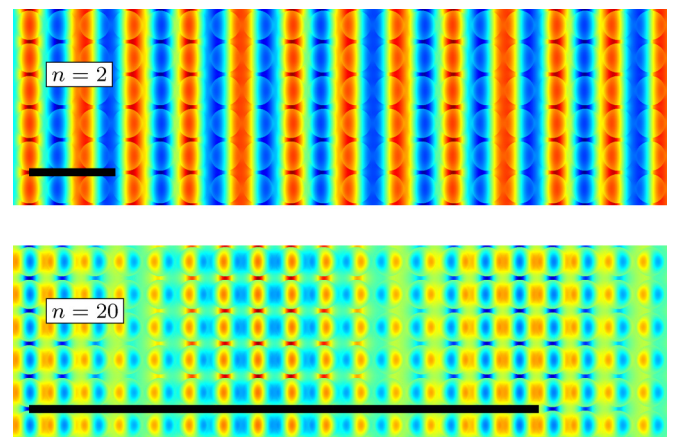


FIG. 8. The transverse field is plotted over an array of 20×6 unit cells to contrast the micro and macroscopic nature of the propagating mode. The black scale bars represent one Floquet wavelength. When $n = 2$, the fields resemble a pure higher order wave, while when $n = 20$ the Floquet wave can be seen in the background of the dominant higher order mode.

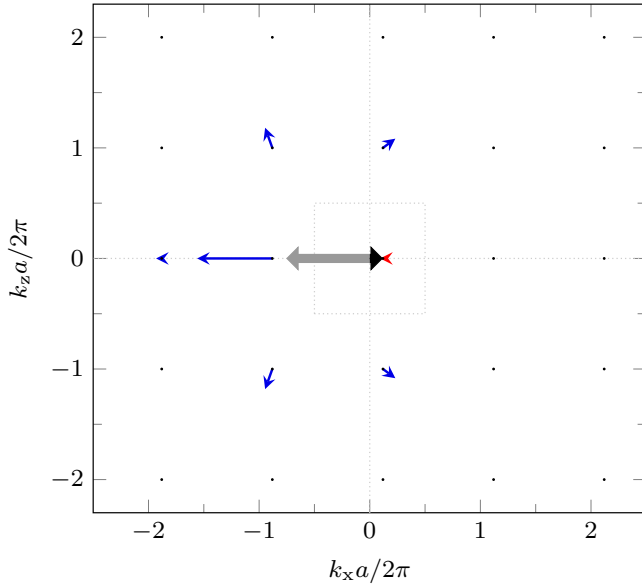


FIG. 9. The mapping of phase and power flow to k space for a lattice of spheres with diameter $d = 0.9a$, permittivity $\epsilon_r = 13.8$, and permeability $\mu_r = 11$. Blue arrows indicate Poynting vectors of left-handed Fourier components, while red arrows indicate those of right-handed components. The thick gray arrow represents the total power, while the short black arrow indicates the Floquet wave vector. The first Brillouin zone is indicated by the dashed square.

V. SPHERICAL MAGNETODIELECTRIC INCLUSIONS

The magnetodielectric sphere medium is the 3D analog to the 1D layered medium and the 2D cylinder medium. It was introduced in 2003 by Holloway *et al.* and was shown to exhibit a negative effective index of refraction that was quasi-isotropic in three dimensions [34]. In subsequent numerical studies, this medium was used to perform many electromagnetic wave manipulation functions associated with left-handed media such as negative refraction and concave lens focusing [32]. With the commercial availability of doped ferrite powders that can provide a magnetodielectric response [35], this medium is a promising candidate for realizing practical bulk negative index metamaterials.

The application of homogenization techniques to the MD sphere medium produces negative effective permittivity and permeability that suggest the medium is left-handed [15,36,37]. Mapping phase and power flow in k space, however, reveals a more complicated relationship in which power is distributed across multiple components surrounding the $m = -1$ component. This spectral power distribution closely resembles that of the array of cylinders from Sec. IV and reflects the similarities between corresponding field distributions. In both cases, the fields within the inclusions propagate in the negative x direction while the fields in air propagate in the positive x direction. As with the 2D periodic layers, the power spectrum of the 3D spheres does not approach that of an ideal homogeneous left-handed medium. The finite transverse extent of the spheres enables the wave to flow around the inclusions when the inclusions are small, preventing the fundamental mode from dominating the power spectrum. Figure 9 plots the power flow in k space for the

magnetodielectric-sphere structure composed of spheres of diameter $d = 0.9a$, permittivity $\epsilon_r = 13.8$, and permeability $\mu_r = 11$. Here the matched condition of the spheres was relaxed slightly so that the electromagnetic properties of real doped ferrite powders could be studied. When the spheres are immersed in air with a lattice constant $a = 0.119\lambda$, the electromagnetic wave propagates with a Floquet wave vector that is equal in magnitude but opposite in sign to that of free space [32].

Although the fundamental Fourier component of the propagating mode is left-handed (indicated by a red arrow), it carries very little of the total power. The largest power contribution comes from the $(m_x, m_y, m_z) = (-1, 0, 0)$ mode outside the first Brillouin zone. This mode is right-handed (indicated by a blue arrow) and arises from the compressed wave propagating backwards through the MD spheres. Other right-handed components are present, distributed symmetrically about the x axis, and providing a very small net contribution to the total power.

The mechanism of field compression can provide opposing power flow and Floquet phase propagation in 3D MD sphere metamaterials, however, most of the power is carried in high-order components and the power spectrum will never be congruent with that of a pure left-handed medium.

VI. CONCLUSION

The relationship between phase and power flow in a medium of magnetodielectric layers has been investigated. As the layer periodicity and the MD fill factor decreases, the spectral power response was shown to approach that of an ideal homogeneous left-handed medium. The fraction of power contained within the fundamental Fourier component, which is of great interest since it has the same propagation constant as the homogeneous effective medium representation, can be made arbitrarily close to unity. This produces a complete spectral congruence with an ideal homogeneous medium—a result that, to the best of our knowledge, has never been observed in other metamaterials. Furthermore, left-handedness within this metamaterial occurs without negative electric or magnetic susceptibility, relying instead on field compression within the MD layers.

It was shown that a nonmagnetic structure will never exhibit pure left-handedness due to the right-handedness of all Fourier components. Cylindrical and spherical inclusions also do not produce pure left-handedness. Backward Floquet waves are supported when the fill ratio of the inclusions is large (typically larger than $a/2$), however, under this condition the dominant Fourier component in k space is located outside the first Brillouin zone and is right-handed.

The complete mapping of phase and power to k space has been shown to provide new insights into the nature of wave propagation within periodic structures and metamaterials. The multidimensional representation of power flow in the spatial frequency domain contributes to the generalization of handedness to heterogeneous structures and provides a complete description of the electromagnetic fields without discarding any information through sampling or averaging. In this paper, metamaterials composed of periodic

magnetodielectric inclusions were studied, providing clues towards the origin of left-handedness and backward waves. Further research on electromagnetic wave propagation through other negative-refractive-index metamaterial structures is forthcoming.

ACKNOWLEDGMENTS

I would like to thank Kenneth Chau for many stimulating discussions on this topic. This work has been supported by CMC Microsystems and the Natural Science and Engineering Council of Canada (NSERC) Discovery Grant Program.

-
- [1] V. G. Veselago, *Sov. Phys. Usp.* **10**, 509 (1968).
- [2] I. V. Lindell, S. A. Tretyakov, K. I. Nikoskinen, and S. Ilvonen, *Microw. Opt. Technol. Lett.* **31**, 129 (2001).
- [3] G. V. Eleftheriades and K. G. Balmain, *Negative-Refractive Metamaterials: Fundamental Principles and Applications* (Wiley-IEEE Press, Hoboken, 2005).
- [4] R. A. Shelby, D. Smith, and S. Schultz, *Science* **292**, 77 (2001).
- [5] G. V. Eleftheriades, A. K. Iyer, and P. C. Kremer, *IEEE Trans. Microwave Theory Tech.* **50**, 2702 (2002).
- [6] N. Engheta and R. W. Ziolkowski, *Metamaterials: Physics and Engineering Explorations* (Wiley-IEEE Press, New York, 2006).
- [7] M. Kafesaki, I. Tsiapa, N. Katsarakis, T. Koschny, C. M. Soukoulis, and E. N. Economou, *Phys. Rev. B* **75**, 235114 (2007).
- [8] T. Xu, A. Agrawal, M. Abashin, K. J. Chau, and H. J. Lezec, *Nature (London)* **497**, 470 (2013).
- [9] S. Foteinopoulou, *Phys. B* **407**, 4056 (2012).
- [10] M. Beruete, M. Sorolla, and I. Campillo, *Opt. Express* **14**, 5445 (2006).
- [11] A. Mary, S. G. Rodrigo, F. J. Garcia-Vidal, and L. Martin-Moreno, *Phys. Rev. Lett.* **101**, 103902 (2008).
- [12] S. Foteinopoulou and C. M. Soukoulis, *Phys. Rev. B* **72**, 165112 (2005).
- [13] D. R. Smith and J. B. Pendry, *J. Opt. Soc. Am. B* **23**, 391 (2006).
- [14] M. G. Silveirinha, *Phys. Rev. B* **75**, 115104 (2007).
- [15] A. Alù, *Phys. Rev. B* **84**, 075153 (2011).
- [16] I. Tsukerman and V. A. Markel, *Proc. R. Soc. A* **470**, 20140245 (2014).
- [17] J. B. Pendry, A. J. Holden, W. J. Stewart, and I. Youngs, *Phys. Rev. Lett.* **76**, 4773 (1996).
- [18] J. B. Pendry, A. J. Holden, D. J. Robbins, and W. J. Stewart, *IEEE Trans. Microwave Theory Tech.* **47**, 2075 (1999).
- [19] D. R. Smith, W. J. Padilla, D. C. Vier, S. C. Nemat-Nasser, and S. Schultz, *Phys. Rev. Lett.* **84**, 4184 (2000).
- [20] V. M. Shalaev, W. Cai, U. K. Chettiar, H.-K. Yuan, A. K. Sarychev, V. P. Drachev, and A. V. Kildishev, *Opt. Lett.* **30**, 3356 (2005).
- [21] A. K. Iyer and G. V. Eleftheriades, *J. Opt. Soc. Am. B* **23**, 553 (2006).
- [22] G. Shvets and Y. A. Urzhumov, *J. Opt. A Pure Appl. Opt.* **7**, S23 (2005).
- [23] G. Shvets, *Phys. Rev. B* **67**, 035109 (2003).
- [24] M. Beruete, P. Rodriguez-Ulibarri, V. Pacheco-Peña, M. Navarro-Cía, and A. E. Serebryannikov, *Phys. Rev. B* **87**, 205128 (2013).
- [25] I. Aghanejad, K. J. Chau, and L. Markley, in *IEEE International Symposium on Antennas and Propagation and USNC/URSI National Radio Science Meeting, Vancouver, BC, 2015* (IEEE, Piscataway, 2015), pp. 657–658.
- [26] M. Notomi, *Opt. Quantum Electron.* **34**, 133 (2002).
- [27] See www.comsol.com.
- [28] L. Brillouin, *Wave Propagation in Periodic Structures* (Dover Publications, New York, 1953).
- [29] B. Lombardet, L. A. Dunbar, R. Ferrini, and R. Houdré, *J. Opt. Soc. Am. B* **22**, 1179 (2005).
- [30] M. H. Al Shakhs, P. Ott, and K. J. Chau, *J. Appl. Phys.* **116**, 173101 (2014).
- [31] R. Maas, E. Verhagen, J. Parsons, and A. Polman, *ACS Photon.* **1**, 670 (2014).
- [32] X. X. Liu and A. Alù, *Metamaterials* **5**, 56 (2011).
- [33] M. Zedler and G. V. Eleftheriades, *IEEE Trans. Microwave Theory Tech.* **58**, 1521 (2010).
- [34] C. L. Holloway, E. F. Kuester, J. Baker-Jarvis, and P. Kabos, *IEEE Trans. Antennas Propag.* **51**, 2596 (2003).
- [35] See www.trans-inc.com or www.magneticsgroup.com.
- [36] A. A. Krokhnin and E. Reyes, *Phys. Rev. Lett.* **93**, 023904 (2004).
- [37] R. A. Shore and A. D. Yaghjian, *Proceedings of the European Conference on Antennas and Propagation (EuCAP), Nice, France, 6-10 November 2006*, Vol. 626 (European Space Agency, The Netherlands, 2006).